

Magnetically Responsive Melt Electrowritten Structures

Paula G. Saiz,* Ander Reizabal, Simon Luposchinsky, Jose Luis Vilas-Vilela, Senentxu Lanceros-Mendez, and Paul D. Dalton*

While melt electrowriting (MEW) can result in complex microstructures, research demonstrating such fabrication with active materials is limited. Herein, magneto-responsive poly(ϵ -caprolactone) (PCL) inks containing up to 10 wt% of iron-oxide (Fe_3O_4) nanoparticles are used to produce fiber with diameters of $9.2 \pm 0.6 \mu\text{m}$ in ordered microstructures when processed by MEW. Introducing the Fe_3O_4 nanoparticles has a minimal overall effect on printing quality compared to pure PCL under similar conditions. The magnetic response of Fe_3O_4 containing fibers allows magnetic actuation, which is one of the first steps to control movement in such structures. Printed samples show different magnetic responses that can be controlled by the micro- and macro-structure design, the nanoparticle concentration, and multi-material design. The potential of MEW to print active magnetic complex micro- and macro-structures for 4D printing designs is demonstrated, in which active properties can be further tailored with magneto-responsive fillers with varying characteristics and by changing MEW fiber diameters.

1. Introduction

Additive manufacturing (AM), also referred as 3D printing, is used to solve challenges across many applications and fields.^[1–3] It produces reproducible structures with flexible designs, including geometries that cannot be obtained in any other way.^[4] Adapting to specific applications and requirements, different AM techniques have rapidly emerged in recent years, each with its own strengths and weaknesses, and covering different printable materials.^[5]

MEW is an electrohydrodynamic AM technology that direct-writes polymeric ultrafine microfibers.^[6] MEW has, in particular, found use for cell invasive scaffolds in biomedical applications such as tissue engineering,^[7] cancer research,^[8] and biofabrication.^[9] MEW employs an electrohydrodynamic effect to deposit

continuous polymeric fibers (with diameters typically ranging between 2 and 50 μm) from the melt onto a collector using direct-writing principles.^[10] The fibers are one or two orders of magnitude smaller than those made from traditional extrusion-based AM technologies including fused filament fabrication (FFF) or 3D bioprinting, with the minimum MEW fiber diameter currently reported being 350 nm.^[11] With the majority of research directed toward implantation or 3D cell culture, MEW has established itself as a promising technique for fabricating scaffolds with a variety of porosities and shapes.^[12–14]

As a young technology, there remain many possible printable “inks” to investigate for MEW, with PCL as the current gold standard.^[15] One interesting class of inks are those that contain functional fillers to provide active properties, which are seldom used in MEW processing.^[16–20] This perspective is important since fillers can hold the key for 4D printing, where structures fabricated with smart materials can be stimulated to change their properties (such shape, size, or color) with time under an external stimulus (such as temperature or light).^[21,22]


In particular, the achievement of motion or shape-changes by means of an external stimulus is a very promising 4D printing approach.^[23] In this context, magnetically responsive samples, able to respond to an external magnetic field by either changing their shape or moving, have shown utility in soft robotics, biomedicine, electronics, and/or actuators, while using safe and simple actuation mechanisms.^[24,25] From this perspective, the shaping of these materials into desired 3D structures that will be later stimulated is a key factor to achieve the desired final actuation characteristics.^[26,27] For that reason, several

P. G. Saiz, A. Reizabal, S. Luposchinsky, P. D. Dalton
Phil and Penny Knight Campus for Accelerating Scientific Impact
University of Oregon
1505 Franklin Boulevard, Eugene, OR 97403, USA
E-mail: paula.gonzalez@ehu.eus; pdalton@uoregon.edu

P. G. Saiz, J. L. Vilas-Vilela
Macromolecular Chemistry Group (LQM)
Physical Chemistry Department
Faculty of Science and Technology
University of the Basque Country
Leioa 48940, Spain

A. Reizabal, S. Lanceros-Mendez
BCMaterials
Basque Center for Materials, Applications, and Nanostructures
Bldg. Martina Casiano
UPV/EHU Science Park
Leioa 48940, Spain

S. Lanceros-Mendez
IKERBASQUE
Basque Foundation for Science
Plaza Euskadi 5, Bilbao 48009, Spain

 The ORCID identification number(s) for the author(s) of this article can be found under <https://doi.org/10.1002/admt.202202063>

© 2023 The Authors. Advanced Materials Technologies published by Wiley-VCH GmbH. This is an open access article under the terms of the Creative Commons Attribution License, which permits use, distribution and reproduction in any medium, provided the original work is properly cited.

DOI: 10.1002/admt.202202063

manufacturing technologies such FFF, stereolithography, inkjet printing, or digital light processing, have been employed and evaluated to design magnetic structures for 4D printing, each with their own advantages and disadvantages, and adapted for different materials.^[28,29] In particular, some disadvantages of those techniques include the need for a solvent, the lack of control over the microstructure, and the difficulties faced when creating multi-material structures, for which other techniques should be explored to introduce new functionalities in this area.^[30]

Herein, the potential of using MEW for printing magnetic responsive structures with controlled features and multi-material designs is evaluated with the aim of introducing this technique within the current available palette of printing techniques. Here, magnetoactive PCL inks containing up to 20 wt% Fe₃O₄ nanoparticles were developed and printed. Well-defined printed samples with up to 5 wt% were able to respond to an external magnetic field depending on the printed structure and the nanoparticle concentration. The potential to design complex and multi-material MEW structures with magnetoactive properties is demonstrated, in a proof of principle approach to highlight the possibilities for the future design of active structures. Furthermore, processing PCL fibers and Fe₃O₄ together brings other perspectives to MEW scaffolds such as magnetic resonance imaging^[31] or hyperthermia^[32] applications.

2. Experimental Section

2.1. Materials

Medical grade PCL was sourced from Corbion (PURASORB PC 12, 2007001461, USA) while magnetite (Fe₃O₄) iron-oxide nanoparticles with an average size of 100 nm and a purity of 99% were purchased from Nanostructured and Amorphous Materials (2651WJ, USA). The Fe₃O₄ nanoparticles were characterized in terms of magnetic and structural properties (Figure S1, Supporting Information). Chloroform from Acros Organic was used as solvent to facilitate mixing. All the materials were used as received.

2.2. Sample Preparation

A total of five PCL blends with different Fe₃O₄ content (0, 1, 5, 10, and 20 wt%) were prepared. For that, 90 min magnetically stirred PCL/chloroform solution (400 mg mL⁻¹) and 90 min sonicated Fe₃O₄/chloroform dispersion, were combined and mixed by sonication (Branson 3800, USA) for a further 30 min and spread onto a glass plate. Films were predried overnight at room temperature and subsequently oven dried for 30 min at 60 °C (Fisherbrand Isotemp, USA) to ensure complete solvent removal. Obtained films were placed in a plastic syringe with a 25-G nozzle (Nordson EFD) and pre-heated at 90 °C for 2 days to fully remove air bubbles. The experimental procedure is schematically shown in Figure 1a and all the samples were referred according to the wt% of Fe₃O₄.

2.3. Melt Electrowriting Printing Process

Fibers were printed using a custom MEW device previously described.^[33,34] Briefly, a print head with electric heating control

contained a syringe that was connected to an adjustable air pressure controller (SMC, USA) and was mounted above a collector with motion controlled by two linear stages (X/Y). A high voltage source was used to generate a voltage difference between the positively charged nozzle and the grounded collector. The MEW printer also had a mandrel collector that swaps with the flat collector.^[35]

A collector distance of 3 mm was set for all the samples and the voltage, temperature, and pressure set to 4.8 kV, 90 °C, and 150 kPa, respectively. The jet speed ranged from 370 to 500 mm min⁻¹ and was determined by measuring the critical translation speed (CTS), where direct-written fiber first deposited in a straight line after increasing the collector speed.^[36] All samples were printed at 1.1× CTS to ensure straight fiber printing while avoiding too much stretching. Different G-codes were generated for the printing of the structures (Figure 1b–g). Printed structures were collected on glass slides or on the metal tubular collectors. Laser cutting into specific shapes was performed with a VLS 2.30 laser cutting machine (Universal Laser Systems, USA).

2.4. Direct Writing Toolpaths

Different toolpaths, in addition to standard 0°/90° square patterns, were designed and printed as shown in Figure 1b–g. Complex microstructures were designed by creating specific G-codes while the overall shape was defined through different approaches: i) by direct toolpath programming for the desired shape (Figure 1b), ii) by cutting post-printing into the desired shape by laser (Figure 1e), or iii) by printing onto a cylindrical mandrel (Figure 1f,g). Furthermore, multi-material structures were made by successive direct writing with different inks (Figure 1c).

2.5. Sample Characterization

The printed samples were characterized by different techniques. The microstructure and morphology were visualized with a digital microscope (VHX-7000, Keyence, USA) and by scanning electron microscopy (SEM) (Apreo 2, Thermo Fisher, USA) equipped with an energy dispersive X-rays (EDX) detector for elemental mapping and chemical analysis. A gold sputtering (Technics Hummer V, USA) coated the printed structures for SEM analysis. Magnetic characterization of the samples was performed with a vibrating sample magnetometer (MicroSense EZ7 VSM, USA) while the magnetic response of the samples was investigated using different neodymium magnets. Finally, a well plate and a Petri dish together with cell culture media were used to demonstrate fixation of scaffolds during media addition. A 60 × 60 mm plate containing nine neodymium magnets of 10 mm in diameter and 2.7 mm in height located in a 3 × 3 configuration was specifically designed and printed by FFF for this experiment.

3. Results

3.1. Printing Ability, Fiber Diameter, and CTS

Initially, the capacity to direct write the PCL/Fe₃O₄ inks using MEW was investigated. To determine the jet speed, successive

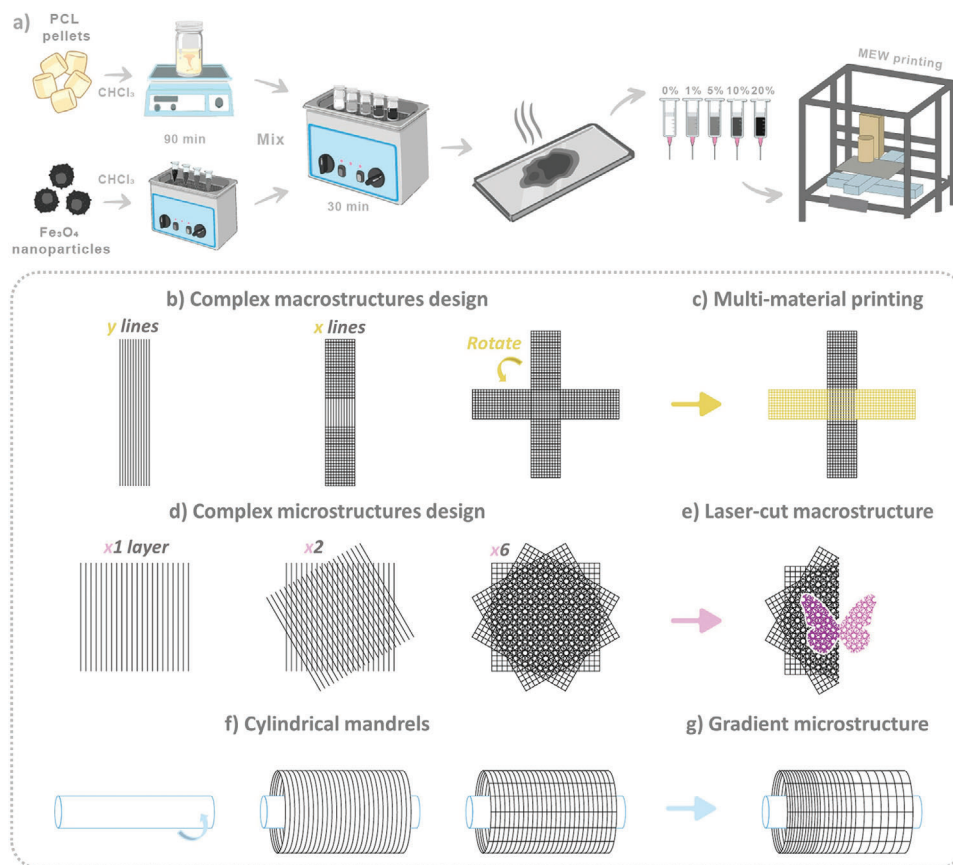


Figure 1. a) Schematic of the sample preparation process. b–g) Schematic of the different printing approaches: b) cross macrostructure including c) multi-material printing, d) mechanically isotropic microstructures, e) laser cut butterfly-shaped macrostructures, f) tubular shapes including g) a gradient microstructure.

straight lines with increasing collector speeds were direct written from 150 to 590 mm min^{-1} in 10 mm min^{-1} increments. All inks could be direct written except the 20 wt% Fe_3O_4 one where the jet broke frequently and/or agglomerated (Figure 2c,d), to the level of not allowing continuous fiber deposition, independent of the parameters used. Continuous fibers could be successfully printed for the 10 wt% ink, however fiber diameter fluctuation occurred (Figure S2a, Supporting Information). This response at higher Fe_3O_4 concentrations could be due to local variations in the viscosity and charge of the inks at these high concentrations due to nanoparticle agglomeration, even visibly observed within the jet during direct writing (Figure 2c). The functionalization of the nanoparticles could be an interesting approach for future investigations to further improve the fillers dispersion, to be able to print at even higher concentrations, and for improving sample biocompatibility.^[16,37]

For the remaining inks (0 , 1 , and 5 wt%), excellent direct writing was observed without jet breakage or noticeable nanoparticle agglomeration (Figure 2a). All samples exhibited typical liquid rope coiling behavior below CTS (Figure 2b) and jet speed progressively decreased from 500 mm min^{-1} for the neat PCL to ≈ 370 mm min^{-1} for the 10 wt% ink (Figure S1c, Supporting Information).

Interestingly, the fiber diameter is almost unaffected by the nanoparticle concentration, exhibiting fiber diameters in the

range of 9.2 ± 0.6 μm for all the inks at the selected printing conditions (Figure 2e and Figure S2a, Supporting Information). The only notable difference in that regard is the larger standard deviation for the fiber diameter with the 10 wt% ink because of the agglomerates observed in that sample. Surprisingly, a recent study on the MEW processing of PVDF/magnetic microparticle blends reported a larger deviation on the fiber diameter/shape which is not observed herein for these concentrations, possibly due to the lower size of the magnetic fillers used in this study.^[38] In line with previously reported PCL results, PCL/ Fe_3O_4 fibers diameter increased at higher processing temperature and pressure, while showing a minor dependence with the voltage (Figure S1d, Supporting Information).^[6,12,39]

The increased nanoparticle content induced a visible darkening in the fiber color to more black (Figure 2e). The progressive drop in surface light reflection and wrinkles, visible by polarized light and SEM, respectively, suggest that the nanoparticles hinder PCL chain nucleation, increasing the content of amorphous domains (Figure 2f). EDX analysis confirmed the presence of the Fe_3O_4 fillers in the samples and relates the increase of dots on the fiber surface with the distribution of the nanoparticles along the fiber and certain nanoparticles agglomerations (Figure S2c, Supporting Information). An effect that is especially visible for 10 wt% samples. Finally, the VSM results confirm the magnetization of the printed samples as a function of the applied magnetic

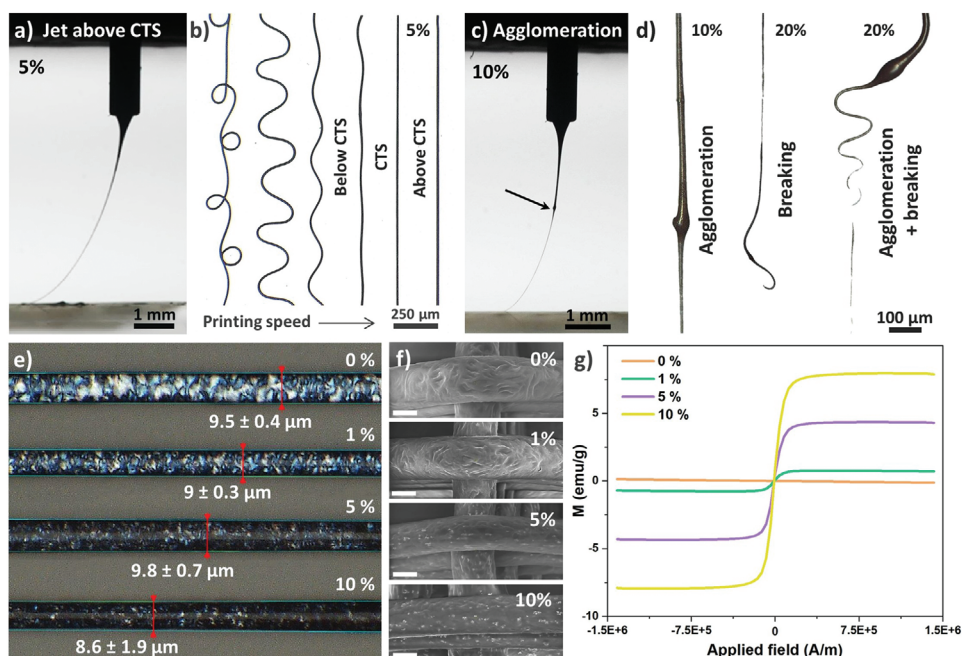


Figure 2. a) Photographs of the MEW jet during the printing process with the 5% sample above CTS, b) optical microscope image of fibers obtained when printing with the 5 wt% ink at different increasing collector speeds, c) image of the jet with visible agglomeration defect for the 10 wt% sample, d) optical microscope images of the agglomeration and breaking observed in the 10 and 20 wt% printed fibers. e) Optical microscope images of the fibers printed for the different inks, f) SEM images of the fiber morphologies with different Fe_3O_4 content (Scale bar = 5 μm). g) B–H curve of the 20 layers printed samples with different nanoparticle concentration.

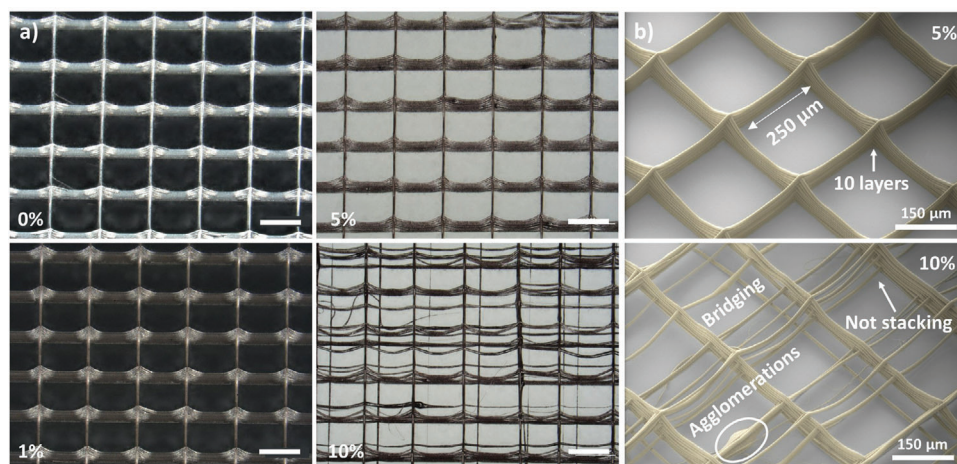


Figure 3. a) Optical microscope images of 20-layer samples with a fiber spacing of 250 μm and increasing Fe_3O_4 content (Scale bar = 200 μm). b) False-colored SEM images detailing the primary differences observed between the 5 and 10 wt% samples.

field (B–H curve), and a direct correlation of samples magnetization with the theoretical nanoparticles content (Figure 2g).^[40]

3.2. Fiber Spacing and Stacking

After the initial characterization, a deeper analysis on the printability of the different samples (0, 1, 5, and 10 wt%) was performed in terms of minimum fiber spacing and fiber stacking. For that, 20 × 20 mm square shapes with 0°/90° laydown patterns

and different fiber spacing (150, 200, and 250 μm) were direct written. These samples were also prepared with different layer counts (2, 10, and 20 in total) to investigate possible instabilities that can occur with increased sample heights.^[41] All the samples look similar macroscopically, except the 10 wt% ink where printing defects can be seen for all fiber spacings.

Optical microscopy (shown here just for 250 μm /20 layers [Figure 3a], 150 μm /20 layers [Figure S2b, Supporting Information], and 250 μm /2 layers [Figure S2a, Supporting Information]) shows noticeable differences between the samples. First,

well-defined structures, with constant and uniform square pores, were observed above 250 μm of spacing, and up to 5 wt% of Fe_3O_4 (Figure 3). Below 200 μm spacing, some defects and fiber misplacements arise as result of jet interaction with the previously deposited fibers. Instabilities are more pronounced as the filler content increases and the interspacing decreases (Figure S2b, Supporting Information).

When viewing the 20-layer samples at an angle of 30° (Figure 3a and Figure S2b, Supporting Information), it is observed that the layering accuracy is primarily affected by two factors: i) the fiber spacing and ii) the quantity of Fe_3O_4 nanoparticles. When the fiber spacing is 150 μm , all the samples demonstrated some fiber bridging. This effect decreases when increasing to 200 μm where almost no bridging is observed, and it completely disappears for the 250 μm spacing in the samples with up to 5 wt%. Nevertheless, defects with the 10 wt% samples persist (Figure 3b), likely due to agglomeration and the effect this has on layering, for which these samples are omitted for the rest of this study. Furthermore, the 250 μm fiber spacing is selected as the standard fiber spacing to investigate more complex magnetic structures.

3.3. Magnetic Responsive Structures

Having determined that the 1 and 5 wt% Fe_3O_4 inks provide good fiber placement and enough magnetic signal, more complex structures were designed, from the perspective of shape and magnetic response possibilities (Figure 1b–g). Since the mechanical response of MEW samples is affected by the fiber placement, both shape control and heterogeneous Fe_3O_4 regions were used to demonstrate their magnetic response. The increased flexibility of the smaller diameter fibers printed by MEW in comparison with those printed by FFF highlights the main advantage of MEW, as described in the next section, and warrants further investigation of the potentials of these microstructures for magnetic actuation.

3.3.1. Relationship between the Second Moment of Area and Volume of a Fiber

MEW readily surpasses the resolution limits of several AM technologies, which is why its potential in 4D printing should be explored, exploiting the increased flexibility that smaller diameter fibers inherently possess. Fibers obtained by techniques such FFF (around 100 μm) are thicker than that obtained by MEW (around 10 μm) and hence would be stiffer and suffer less displacement under an external force (such as a magnetic field). This increased fiber flexibility is a result of the second moment of area (I), which strongly decreases with a reduction in fiber diameter. For a pinned beam representing a fiber spanning two points, the maximum displacement (δ) under a force (F) is approximated by Equation (1):^[42]

$$\delta = \frac{FL^3}{48EI} \quad (1)$$

where E is the elastic modulus, L is the length of the beam, and I is the second moment of area. The relation of I for cylindrical

fibers to their fiber diameter (d) can be expressed as:^[43]

$$I = \frac{\pi d^4}{64} \quad (2)$$

As a result, the smallest fiber struts obtained by techniques such as FFF (100 μm fibers; $I = 4\,910\,000\ \mu\text{m}^4$) are stiffer and hence displace less under an external force than the diameters obtained here using MEW (10 μm fibers; $I = 491\ \mu\text{m}^4$).

Furthermore, the magnetic deflection would depend on the mass of magnetic material and hence on the fiber volume. The volume (V) of a cylinder is described by Equation (3):

$$V = L\pi r^2 \quad (3)$$

The volume of FFF printed fibers is higher but reduces significantly less with the fiber diameter than the second moment of area does, as can be seen in Figure S3, Supporting Information. This highlights the importance of defined, well-placed small diameter fibers for actuation as they become more flexible while retaining a certain volume/mass that is required to drive their deflection. The benefit of using smaller diameter fibers for some 4D printing strategies is clear because forces required for their deflection and bending are significantly reduced, while a certain volume is retained to drive actuation.

3.3.2. Multi-Material Cross-Shape Macrostructures for Grip Response

To investigate magnetic response, different specific macrostructure shapes together with microstructures were defined during printing, and multi-material printing (with different amounts of Fe_3O_4) was also explored. Cross-shaped macrostructures were first selected to show magnetic actuation response. Using a 0°/90° laydown pattern (250 μm interspace), samples with different sizes and number of layers were designed and printed. Cross-shaped structures of 45 mm in length, 10 mm “arms,” and a total of 40 layers (Figure S4, Supporting Information) were first printed with the different inks (0, 1, and 5 wt%). The magnetic response (Video S1 and Figure S4, Supporting Information) shows that the 5 wt% samples readily grip the magnet when it approaches while the 1 wt% sample response is weaker and 0% samples do not show any response, as expected.

Based on previous outcomes, and to show the multi-material printing ability and its potential to adapt the magnetic response of samples, pure PCL (unresponsive fibers) and 5 wt% Fe_3O_4 (responsive) inks were also mixed within smaller cross-shape microstructures (Figure 4a) and tested as magnetic grips with controlled response (Video S2, Supporting Information). Details of this multi-material structure can be seen in Figure 4b where the responsive and unresponsive fibers intersect. The distinct surface spots on the upper layers (false-colored yellow) are indicative of the responsive fibers that contain nanoparticles. The direct writing is performed sequentially, so fibers are not interlocked at intersections. Programming actuation is a fundamental concept that, as demonstrated here, could be achieved by MEW with only selected arms made from responsive fibers in this mixed sample being deflected as the magnet approached the sample (Figure 4c and Video S2, Supporting Information).

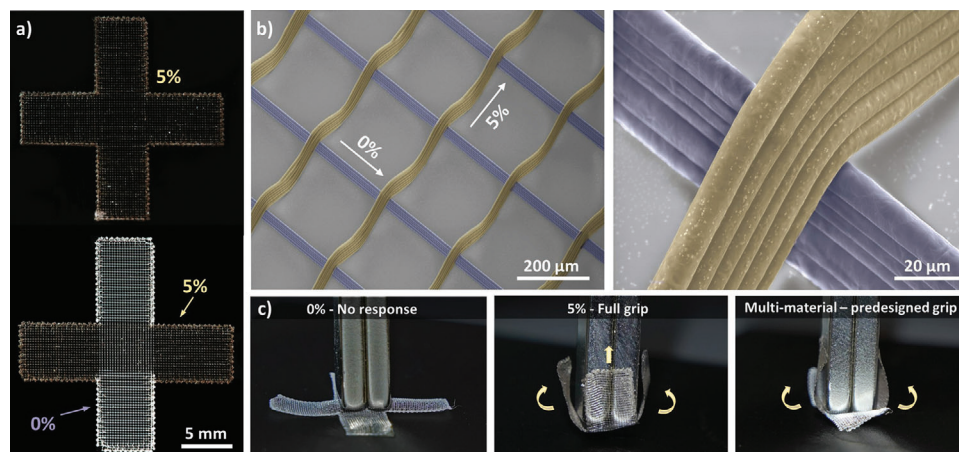


Figure 4. a) Images of small cross-shaped samples with a $0^\circ/90^\circ$ microstructure (20 mm in length and 5 mm width arms with a total of 12 layers) with 5% Fe_3O_4 and a mix of PCL + 5% Fe_3O_4 inks. b) False-colored SEM images of the fiber intersections in the multi-material sample. c) Photographs of the cross-shaped samples deflected under an external magnetic field (Video S2, Supporting Information).

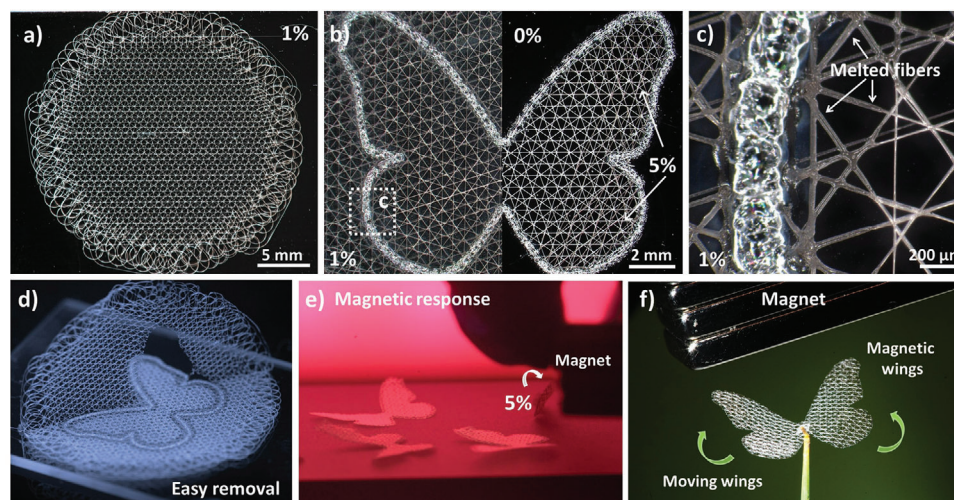


Figure 5. a–d) Photographs of laser cutting into a butterfly shapes. a) Mechanically isotropic MEW microstructure with $0^\circ/30^\circ/60^\circ/90^\circ/120^\circ/150^\circ$ laydown pattern (1 wt%). b) Laser-cut butterfly-shaped samples for the 1 wt% ink (left), overlaid with images from a mixed 0 and 5 wt% multi-material sample (right). c) Detail of the laser cut edge but also of fibers melting nearby ultimately allowing d) facile removal of the desired shape. e, f) Magnetic response of the printed + cut samples: e) 5 wt% samples getting attracted to the magnet and f) wings moving up and down on the multi-material sample when approaching the magnet (Video S3, Supporting Information).

3.3.3. Isotropic Microstructures on Butterfly-Shape Macrostructures

Laser-cut samples were used to further demonstrate how programming actuation can be implemented by the overall shape. In this instance, a mechanically isotropic microstructure with a $0^\circ/30^\circ/60^\circ/90^\circ/120^\circ/150^\circ$ laydown pattern (Figure 1d) and a total of 60 layers (Figure 5a) was used as a base microstructure. Similar to previous observations, no appreciable geometric differences between the magnetic and non-magnetic samples are observed (Figure S5, Supporting Information). Using this microstructure, a butterfly-shaped macrostructure was defined by a laser cut (Figures 1e and 5b). This method produced a clear-cut shape with notable partial fiber melting around the edges (Figure 5c), which allowed facile post-cutting removal and effectively fused the fibers around the edge (Video S3, Supporting Informa-

tion, and Figure 5d). Both the macroscopic shape and microstructure are expected to influence the flexible behavior that is induced by magnetic actuation. To further demonstrate the potential of this technique, a multi-material butterfly-shape fully made of PCL 0 wt% ink and only two small regions with 5 wt% ink deposited along the wings area was designed (Figure 5b [right]). The fiber fusion of laser cutting ensured that the different fiber materials are well joined—another advantage of using this technique that avoids having to alternate layers to ensure both materials do not delaminate.

The actuation response of the samples toward a magnet (Video S3, Supporting Information) was initially shown by varying its proximity. The 5 wt% samples lifted off onto the magnet when it is ≈ 1.5 cm away (Figure 5e) while the 1 wt% ink samples just showed a small movement only when the magnet is millimeters

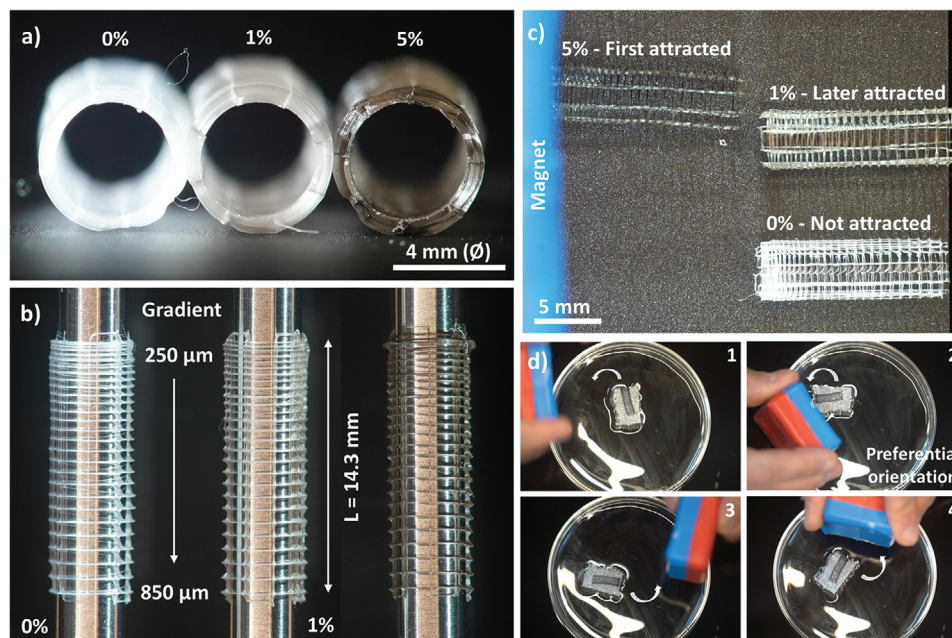


Figure 6. a,b) Photographs of the tubes with gradient features and 0, 1, and 5 wt% of Fe_3O_4 : a) viewing into the lumen (ID = 4 mm) and b) samples on the mandrel ($L = 14.3$ mm). c,d) Movement response of designed tubes toward an external magnetic field (Video S5, Supporting Information): c) different response with distance and wt% and d) constant rotation of the 5 wt% Fe_3O_4 toward a preferential orientation facing the magnet from the side with higher mass accumulation.

away. These results demonstrate that a concentration of 5 wt% and even of 1 wt% is enough to show a magnetic response and that it is possible to control the strength of the magnetic response varying the concentration of the magnetic fillers. Moreover, the magnetic response of the multi-material butterfly shape was cyclically tested (Figure 5f) in the presence of a magnetic field of varying intensity (moving magnet). Video S3, Supporting Information, shows how the wings bend toward the magnet and move in a controlled way depending on the magnet position. The magnetic response, while sufficient here for movement, could be further tuned by using magnetic fillers of higher magnetization or by increasing filler concentrations, leading to high potential 4D printing designs where a response in just specific zones can be designed.^[44,45]

3.3.4. Non-Planar Collectors—Gradual Tubular Structures with Preferential Orientation

While not as common as flat collectors, MEW can be also performed onto mandrels, which extend the manufacturable range of printed structures.^[35,46] Thus, tubular structures with a gradient on the microstructure, and hence on the magnetic mass amount, were fabricated for the different nanoparticle concentrations as another example of magnetic MEW potential. Tubes with an internal diameter (ID) of 4 mm, 14.3 mm in length (L), and a total of 40 layers were fabricated. Their design consists of high-pitch fiber winding with decreasing radial fiber spacing from 850 to 250 μm in 50 μm steps with two repetitions for each spacing. These samples are structurally reinforced with eight longitudinally placed fiber walls. **Figure 6a,b** shows the lateral view (gra-

dient microstructure) and top view of the printed structures with different amounts of nanoparticles. Further detailed imaging is given in Figure S6a, Supporting Information, for 1 wt% sample structure and mechanical properties. It was an effective way to observe fiber bridging defects at this high stacking, which are eliminated as the fiber spacing increases, leading to excellent 40 layers stacking at fiber spacings above 650 μm . The self-standing tubular structures (Figure S6b, Supporting Information) demonstrate recoverable bending properties (Video S4 and Figure S6c,d, Supporting Information).

The different magnetic responses of the tubes are shown in Video S5, Supporting Information. First, the response of the three tubular structures was compared by approaching them with a magnet and measuring the minimum distance before the samples move (Figure 6c). As expected, the tube with the 5 wt% ink has the strongest responsiveness at ≈ 16 mm while the movement of the 1 wt% occurs at ≈ 5.5 mm and the 0 wt% sample is unresponsive to the magnet. Moreover, the direction of the gradient also impacted these values. As shown for the 5 wt% inks, it is observed that the distance at which the samples react to the magnetic force depends on their orientation, and also that they show a preferential orientation, rotating when approaching the magnet from the lower density area or from the tubes side, as a result of the gradient in the mass of magnetic material along the microstructure (Video S5, Supporting Information). This preferential orientation of the tubes was further confirmed by placing the 5% tube above a foam sponge floating in water and approaching a magnet from different sides of the tube (Figure 6d). When further placing samples in water, providing more resistance to tube movement, the tubes are also able to rotate into the preferential orientation as they approach the magnet (Video S5, Supporting

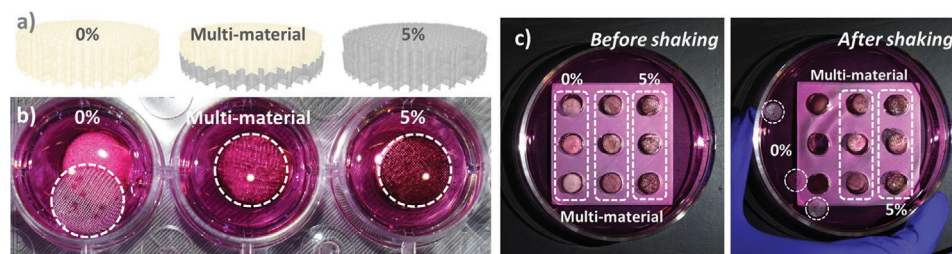


Figure 7. Magnets to adhere scaffolds in cell culture: a) Schematic of the sample design, b) photograph of the different well plates with the magnets configuration underneath and typical movement of the scaffolds after adding the cell media, and c) photograph of the scaffolds located on a Petri dish before and after the shaking process.

Information). In all the cases, the rotation of the tube toward the heavier mass orientation was observed. This magnetic response gives the opportunity to control the position and orientation of the printed structures in different media which could be further combined with other functionalities to promote a multi-active response by multi-material MEW printing.

3.4. Potential Applications of the Magnetic Microstructures: Scaffolds Control in Cell Media

The inherent magnetic properties within the presented MEW scaffolds were leveraged to hold samples within a media dish, relevant for MEW since cell culture is regularly performed within this environment. MEW scaffolds are lightweight and when exposed to cell media in wells, they move and even bend, flip over, or stick to the walls of the culture plates. This makes the experiments variable and affected by each media exchange. The magnetic scaffolds can be anchored with an external magnet underneath a well plate avoiding these arising problems. Taking this into account, three types of scaffolds with a $0^\circ/90^\circ$ laydown pattern with pores of $250\ \mu\text{m}$ and a total of 40 layers were designed with: i) unresponsive fibers (PCL), ii) half unresponsive + half responsive fibers (5 wt%), and iii) fully responsive fibers (Figure 7a). Circular samples 9.5 mm in diameter were laser cut for the experiments and the results shown in Figure 7b,c and Video S6, Supporting Information.

Since the scaffolds are near the magnets, only separated by 1 mm of the dish walls, the movement for even the bilayer scaffolds were diminished (Figure 7b). This improvement is clear when adding the cell media since the neat PCL scaffolds float and move, even adhering to the walls. Contrary, when adding the media to the magnetic scaffolds, and even to the multi-material ones, these remain on the bottom part of the well, near to the place where the magnets are located, without relevant displacement as could be observed in Figure 7b. Moreover, since no ‘flipping’ of the samples is observed, this provides a temporary holding mechanism when a certain scaffold orientation is required. This adhesion was extended to manually shaking Petri dishes (Figure 7c and Video S6, Supporting Information) and could be also extended to different magnet configurations. In a similar and more refined approach, this could be useful for dynamic cell culture of scaffolds containing multi-material components since there are several biological tissues that would benefit from mechanical stimulation during culture.^[47,48]

4. Conclusions

Magnetically responsive structures have been developed by MEW. PCL with up to 5 wt% of Fe_3O_4 magnetic nanoparticles have shown good compatibility with MEW to print well-defined structures, similar to that obtained for the pure PCL. At the higher nanoparticle concentration of 10 wt%, agglomerations affect fiber deposition accuracy and overall sample quality. Samples with higher content of nanoparticles could potentially be printed by functionalizing the nanoparticles to improve their dispersion or by using another type of fillers, which will be the subject of further research in this line.

Samples with 1 and 5 wt% nanoparticles exhibit magnetic responses (shape change or displacement) toward an external magnetic field. Different magnetic responses have been achieved, such as grip response, ‘wings’ flapping, or preferential orientation depending on the predefined macro- and micro-structures, which could be further tuned by using other fillers with greater magnetic response or printing of other structures. The possibility of multi-material printing has been also demonstrated, taking a step forward by improving the complexity of the fabricated structures, and providing new ideas for controlling the active properties of the designed samples by combining different materials with different active responses directly while MEW printing. Finally, the potential of these magnetic structures as supporting scaffolds for controlling the position of MEW scaffolds within cell culture media has been demonstrated, important for cell experiments, potentially with a certain mode of mechanical actuation.

The fundamental demonstration of magnetically actuating MEW scaffolds for fabricating customized stimuli-responsive 4D structures is underpinned in this study. This opens numerous possibilities for complex structure MEW designs at the microscale level using different active fillers combined with the possibilities for multi-material printing. For that purpose, exploring new active materials and fillers for MEW printing should be one of the research focuses around this technology in the future.

Supporting Information

Supporting Information is available from the Wiley Online Library or from the author.

Acknowledgements

The support of the University of the Basque Country (UPV/EHU) for the Margarita Salas postdoctoral grant for P.G.S. under the ‘Convoca-

toria de ayudas para la recualificación del sistema universitario español para 2021–2023” and for the Open Access funding is gratefully acknowledged. The financial support from the Wu Tsai Human Performance Alliance and the Joe and Clara Tsai Foundation is appreciated.

Conflict of Interest

The authors declare no conflict of interest.

Data Availability Statement

The data that support the findings of this study are available from the corresponding author upon reasonable request.

Keywords

actuators, four-dimensional printing, magnetism, melt electrospinning writing, nano-composites, nanoparticles

Received: December 5, 2022

Revised: January 26, 2023

Published online: April 10, 2023

- [1] N. Saengchairat, T. Tran, C.-K. Chua, P. Prototyping, *Virtual Phys. Prototyping* **2017**, *12*, 31.
- [2] M. J. M. Salmi, *Materials* **2021**, *14*, 191.
- [3] B. Blakey-Milner, P. Gradl, G. Snedden, M. Brooks, J. Pitot, E. Lopez, M. Leary, F. Berto, A. J. M. du Plessis, *Mater. Des.* **2021**, *209*, 110008.
- [4] M. K. Niaki, S. A. Torabi, F. Nonino, *J. Cleaner Prod.* **2019**, *222*, 381.
- [5] *3D Printing and Additive Manufacturing Technologies* (Eds: L. J. Kumar, P. M. Pandey, D. I. Wimpenny), Springer, New York **2019**.
- [6] T. D. Brown, P. D. Dalton, D. W. Huttmacher, *Adv. Mater.* **2011**, *23*, 5651.
- [7] G. Weisgrab, O. Guillaume, Z. Guo, P. Heimel, P. Slezak, A. Poot, D. Grijpma, A. Ovsianikov, *Biofabrication* **2020**, *12*, 045036.
- [8] D. Loessner, A. Rockstroh, A. Shokohmand, B. M. Holzapfel, F. Wagner, J. Baldwin, M. Boxberg, B. Schmalfeldt, E. Lengyel, J. A. Clements, D. W. Huttmacher, *Biomaterials* **2019**, *190–191*, 63.
- [9] M. de Ruijter, A. Ribeiro, I. Dokter, M. Castilho, J. Malda, *Adv. Healthcare Mater.* **2019**, *8*, 1970024.
- [10] P. D. Dalton, *Curr. Opin. Biomed. Eng.* **2017**, *2*, 49.
- [11] K. F. Eichholz, I. Gonçalves, X. Barceló, A. S. Federici, D. A. Hoey, D. J. Kelly, *Addit. Manuf.* **2022**, *58*, 102998.
- [12] A. Hrynevich, B. S. Elci, J. N. Haigh, R. McMaster, A. Youssef, C. Blum, T. Blunk, G. Hochleitner, J. Groll, P. D. Dalton, *Small* **2018**, *14*, 1800232.
- [13] I. Liashenko, A. Hrynevich, P. D. Dalton, *Adv. Mater.* **2020**, *32*, 2001874.
- [14] G. Hochleitner, T. Jungst, T. D. Brown, K. Hahn, C. Moseke, F. Jakob, P. D. Dalton, J. Groll, *Biofabrication* **2015**, *7*, 035002.
- [15] J. C. Kade, P. D. Dalton, *Adv. Healthcare Mater.* **2021**, *10*, 2001232.
- [16] L. Pang, N. C. Paxton, J. Ren, F. Liu, H. Zhan, M. A. Woodruff, A. Bo, Y. Gu, *ACS Appl. Mater. Interfaces* **2020**, *12*, 47993.
- [17] J. H. Y. Chung, S. Sayyar, G. G. Wallace, *Polymers* **2022**, *14*, 319.
- [18] A. Abdal-hay, N. Abbasi, M. Gwiazda, S. Hamlet, S. Ivanovski, *Eur. Polym. J.* **2018**, *105*, 257.
- [19] E. Hewitt, S. Mros, M. McConnell, J. D. Cabral, A. Ali, *Biomed. Mater.* **2019**, *14*, 055013.
- [20] K. Somszor, O. Bas, F. Karimi, T. Shabab, N. T. Saidy, A. J. O'Connor, A. V. Ellis, D. Huttmacher, D. E. Heath, *ACS Macro Lett.* **2020**, *9*, 1732.
- [21] X. Kuang, D. J. Roach, J. Wu, C. M. Hamel, Z. Ding, T. Wang, M. L. Dunn, H. J. Qi, *Adv. Funct. Mater.* **2019**, *29*, 1805290.
- [22] Y. Wang, H. Cui, T. Esworthy, D. Mei, Y. Wang, L. G. Zhang, *Adv. Mater.* **2022**, *34*, 2109198.
- [23] A. S. Gladman, E. A. Matsumoto, R. G. Nuzzo, L. Mahadevan, J. A. Lewis, *Nat. Mater.* **2016**, *15*, 413.
- [24] C. Zhang, X. Li, L. Jiang, D. Tang, H. Xu, P. Zhao, J. Fu, Q. Zhou, Y. Chen, *Adv. Funct. Mater.* **2021**, *31*, 2102777.
- [25] A. Reizabal, C. M. Costa, N. Pereira, L. Pérez-Álvarez, J.-L. Vilas-Vilela, S. Lanceros-Méndez, *Adv. Eng. Mater.* **2020**, *22*, 2000111.
- [26] P. Zhu, W. Yang, R. Wang, S. Gao, B. Li, Q. Li, *ACS Appl. Mater. Interfaces* **2018**, *10*, 36435.
- [27] E. Yarali, M. Baniasadi, A. Zolfagharian, M. Chavoshi, F. Arefi, M. Hossein, A. Bastola, M. Ansari, A. Foyouzat, A. Dabbagh, M. Ebrahimi, M. J. Mirzaali, M. Bodaghi, *Appl. Mater. Today* **2022**, *26*, 101306.
- [28] F. Zhang, L. Wang, Z. Zheng, Y. Liu, J. Leng, *Composites, Part A* **2019**, *125*, 105571.
- [29] Y. Zhang, Q. Wang, S. Yi, Z. Lin, C. Wang, Z. Chen, L. Jiang, *ACS Appl. Mater. Interfaces* **2021**, *13*, 4174.
- [30] K. J. Merazzo, A. C. Lima, M. Rincón-Iglesias, L. C. Fernandes, N. Pereira, S. Lanceros-Mendez, P. Martins, *Mater. Horiz.* **2021**, *8*, 2654.
- [31] G. Wang, D. Zhao, N. Li, X. Wang, Y. Ma, *J. Magn. Magn. Mater.* **2018**, *456*, 316.
- [32] J. Zhang, S. Zhao, M. Zhu, Y. Zhu, Y. Zhang, Z. Liu, C. Zhang, *J. Mater. Chem. B* **2014**, *2*, 7583.
- [33] F. M. Wunner, O. Bas, N. T. Saidy, P. D. Dalton, E. M. D.-J. Pardo, D. W. Huttmacher, *J. Visualized Exp.* **2017**, *130*, e56289.
- [34] S. Florczak, T. Lorton, T. Zheng, M. Mrlik, D. W. Huttmacher, M. J. Higgins, R. Luxenhofer, P. D. Dalton, *Polym. Int.* **2019**, *68*, 735.
- [35] E. McColl, J. Groll, T. Jungst, P. D. Dalton, *Mater. Des.* **2018**, *155*, 46.
- [36] S. Loewner, S. Heene, T. Baroth, H. Heymann, F. Cholewa, H. Blume, C. Blume, *Front. Bioeng. Biotechnol.* **2022**, *10*, 896719.
- [37] E. Navarro-Palomares, P. Gonzalez-Saiz, C. Renero-Lecuna, R. Martin-Rodriguez, F. Aguado, D. Gonzalez-Alonso, L. F. Barquin, J. Gonzalez, M. Banobre-Lopez, M. L. Fanarraga, R. Valiente, *Nanoscale* **2020**, *12*, 6164.
- [38] J. C. Kade, E. Bakirci, B. Tandon, D. Gorgol, M. Mrlik, R. Luxenhofer, P. D. Dalton, *Macromol. Mater. Eng.* **2022**, *307*, 2200478.
- [39] F. M. Wunner, J. Maartens, O. Bas, K. Gottschalk, E. M. De-Juan-Pardo, D. W. Huttmacher, *Mater. Lett.* **2018**, *216*, 114.
- [40] C. Mendes-Felipe, A. Garcia, D. Salazar, J. L. Vilas-Vilela, S. Lanceros-Mendez, *Compos., Part C: Open Access* **2021**, *5*, 100143.
- [41] J. Kim, E. Bakirci, K. L. O'Neill, A. Hrynevich, P. D. Dalton, *Macromol. Mater. Eng.* **2021**, *306*, 2000685.
- [42] B. J. Goodno, J. M. Gere, *Mechanics of Materials*, Cengage Learning, Noida, Uttar Pradesh **2012**.
- [43] R. Budynas, K. Nisbett, *Mechanical Engineering Design*, McGraw-Hill Education, New York **2019**.
- [44] V. Q. Nguyen, A. S. Ahmed, R. V. Ramanujan, *Adv. Mater.* **2012**, *24*, 4041.
- [45] C. Zhang, X. Li, L. Jiang, D. Tang, H. Xu, P. Zhao, J. Fu, Q. Zhou, Y. Chen, *Adv. Funct. Mater.* **2021**, *31*, 2102777.
- [46] P. Mieszczanek, T. M. Robinson, P. D. Dalton, D. W. Huttmacher, *Adv. Mater.* **2021**, *33*, 2100519.
- [47] W. L. Stoppel, D. L. Kaplan, L. D. Black III, *Adv. Drug Delivery Rev.* **2016**, *96*, 135.
- [48] N. Wang, *J. Phys. D: Appl. Phys.* **2017**, *50*, 233002.